

**Properties and Physiological Function of Ca^{2+} Dependent K^{+}
Currents in Uniglomerular Olfactory Projection Neurons**

Cathleen Bradler*, Ben Warren*, Viktor Bardos, Sabine Schleicher, Andreas Klein,
and Peter Kloppenburg

Biocenter, Institute for Zoology, and Cologne Excellence Cluster on Cellular Stress
Responses in Aging-Associated Diseases (CECAD), University of Cologne, Zùlpicher
Str. 47b, 50674 Cologne, Germany

*Authors contributed equally to this work

Running head: Ca^{2+} dependent K^{+} currents of olfactory projection neurons

Peter Kloppenburg
University of Cologne
Biocenter
Zùlpicher Str. 47b
50674 Cologne, Germany
peter.kloppenburg@uni-koeln.de

ABSTRACT

Ca²⁺-activated potassium currents ($I_{K(Ca)}$) are an important link between the intracellular signaling system and the membrane potential, which shapes intrinsic electrophysiological properties. To better understand the ionic mechanisms that mediate intrinsic firing properties of olfactory uniglomerular projection neurons (uPNs), we used whole-cell patch clamp recordings in an intact, adult brain preparation of the male cockroach *Periplaneta americana* to analyze $I_{K(Ca)}$. In the insect brain uPNs form the principal pathway from the antennal lobe to the protocerebrum, where centers for multimodal sensory processing and learning are located. In uPNs the activation of $I_{K(Ca)}$ was clearly voltage and Ca²⁺ dependent. Thus, under physiological conditions $I_{K(Ca)}$ is strongly dependent on the Ca²⁺ influx kinetics and on the membrane potential. The biophysical characterization suggests that $I_{K(Ca)}$ is generated by BK channels. An SK channel generated current could not be detected. $I_{K(Ca)}$ was sensitive to charybdotoxin and iberiotoxin but not to apamin. The functional role of $I_{K(Ca)}$ was analyzed in occlusion experiments under current clamp, in which portions of $I_{K(Ca)}$ were blocked by charybdotoxin or iberiotoxin. Blockade of $I_{K(Ca)}$ showed that $I_{K(Ca)}$ contributes significantly to the intrinsic electrophysiological properties such as the action potential waveform and membrane excitability.

KEYWORDS: Antennal lobe, chemosensory, glomerulus, olfaction, *Periplaneta americana*

56 INTRODUCTION

57 In insects odors are detected by antennal sensory neurons and are initially processed
58 in the first synaptic relay, the antennal lobe (AL), which is the functional equivalent of the
59 mammalian olfactory bulb (reviewed in Bargmann 2006; Davis 2004; Galizia and Rössler
60 2010; Hildebrand and Shepherd 1997; Strausfeld and Hildebrand 1999; Vosshall and
61 Stocker 2007; Wilson and Mainen 2006). The integrated olfactory information is then
62 conveyed to higher order processing centers in the protocerebrum by antennal lobe
63 projection neurons (PNs), the analog of the mammalian mitral/tufted cells (Su et al. 2009).
64 The most prominent and most studied group of PNs are the uniglomerular projection neurons
65 (uPNs), whose morphology and response properties are well described in various insect
66 species. uPNs are considered the only cholinergic input to the mushroom body calyx (Fusca
67 et al. 2013; Yasuyama et al. 1995, 2002). Typically, each uPN receives synaptic input from
68 olfactory sensory neurons and local interneurons in a single AL glomerulus. Each uPN sends
69 an axonal projection into the mushroom body calyx and/ or the lateral horn where it
70 terminates with synaptic boutons. The tuning profiles and odor responses of uPNs are
71 determined by synaptic inputs from the sensory and local interneurons together with their
72 intrinsic electrophysiological properties. A given uPN can respond to odorants of many
73 different chemical classes, typically with odor specific elaborate patterns of excitation and
74 spiking that could also include periods of inhibition (Broome et al. 2006; Christensen et al.
75 1998; Kanzaki et al. 1989; Lemon and Getz 1998; Mazor and Laurent 2005; Stopfer et al.
76 2003; Watanabe et al. 2012; Wilson et al. 2004).

77 While the odor response profiles of uPNs are generally well documented we have
78 only limited information about the intrinsic firing properties and the cellular mechanisms that
79 determine them. However, in depth knowledge of the cell-type specific intrinsic
80 electrophysiological properties and the membrane conductances that mediate them is an
81 important prerequisite towards a detailed understanding of the cellular basis of olfactory
82 information processing. Here we analyzed the Ca^{2+} dependent K^+ outward currents ($I_{\text{K(Ca)}}$) of
83 uPNs, which play a crucial role in controlling action potential waveform and neuronal

84 excitability (Adelman et al. 2012; Berkefeld et al. 2010; Faber and Sah 2003; Ghatta et al.
85 2006; Greffrath et al. 2004; Vergara et al. 1998).

86 Since Ca^{2+} is an important messenger of the intracellular signaling system, Ca^{2+}
87 dependent ion channels constitute an important link between the intracellular status of
88 neurons and their membrane potential. Vertebrates and invertebrates express several types
89 of Ca^{2+} dependent potassium (K_{Ca}) channels in most neuron types, where they mediate Ca^{2+}
90 dependent hyperpolarization and contribute to the resting membrane potential, spike wave
91 form, and spike frequency. Historically, three main types of K_{Ca} channels have been
92 categorized by their biophysical and pharmacological properties: 1) small conductance (SK)-,
93 2) intermediate conductance (IK)-, and 3) big conductance (BK or maxi K) channels
94 (Adelman et al. 2012; Berkefeld et al. 2010; Faber and Sah 2003). Molecular cloning helped
95 to reveal sequence relationships and made structure/function studies possible (Sah and
96 Faber 2002; Stocker 2004). The SK family has three members ($\text{K}_{\text{Ca}2.1-2.3}$) and is closely
97 related with the IK channel ($\text{K}_{\text{Ca}3.1}$). These channels are activated by cytosolic Ca^{2+} and are
98 not voltage-sensitive. Their activation by intracellular Ca^{2+} is mediated by calmodulin that is
99 constitutively bound to the C-terminus. In contrast, the BK channel ($\text{K}_{\text{Ca}1.1}$) is activated by
100 both voltage and cytosolic Ca^{2+} . The activation by Ca^{2+} is not calmodulin dependent but
101 mediated directly by cytoplasmic Ca^{2+} binding sites (Berkefeld et al. 2010; Fakler and
102 Adelman 2008; Grunnet and Kaufmann 2004; Lee and Cui 2010; Salkoff et al. 2006).

103 Here we aimed to characterize Ca^{2+} dependent K^{+} currents $I_{\text{K(Ca)}}$ of uPNs in the AL of
104 the cockroach *Periplaneta americana*. First, we characterized the general functional
105 properties of $I_{\text{K(Ca)}}$ in uPNs with whole-cell voltage clamp recordings in an intact brain
106 preparation. Second, we used occlusion experiments, in which portions of $I_{\text{K(Ca)}}$ were
107 pharmacologically blocked, to better understand the functional role of $I_{\text{K(Ca)}}$ in shaping the
108 electrophysiological properties of uPNs.

109

110

METHODS

Preparation

P. americana were reared in crowded colonies at 27 °C under a 12 : 12 h light/ dark photoperiod regimen, on a diet of dry rodent food, oatmeal, and water. All experiments were performed with adult males. Chemicals, unless stated otherwise, were obtained from Applichem (Darmstadt, Germany) or Sigma-Aldrich (Taufkirchen, Germany) and were of 'pro analysis' grade. The intact brain preparation was based on an approach described previously (Husch et al. 2009; Kloppenburg et al. 1999a), in which the entire olfactory network was left intact. Animals were anaesthetized by CO₂, placed in a custom built holder, and the head was immobilized with tape (Tesa ExtraPower Gewebefix, Tesa, Hamburg, Germany). The head capsule was opened by cutting a window between the two compound eyes at the bases of the antennae. The brain was dissected in extracellular saline (see below) and pinned in a Sylgard-coated (Dow Corning Corp., Midland, Michigan, USA) recording chamber. To minimize synaptic input to AL neurons, the antennae were removed. To gain access to the recording site and to facilitate the penetration of pharmacological agents into the tissue, we desheathed parts of the AL using fine forceps. Some preparations were also enzymatically treated with a mixture of papain (0.3 mg·ml⁻¹, P4762, Sigma) and L-cysteine (1 mg·ml⁻¹, 30090, Fluka) dissolved in 'normal' saline (~ 2 min, 37°C). For electrophysiological recordings, the somata of the AL neurons were visualized with a fixed stage upright microscope (BX51WI, Olympus, Hamburg, Germany) using a water-immersion objective (UMPLFL, 40x, 0.8 numerical aperture [NA], 3.3 mm working distance, Olympus) and infrared differential interference contrast optics (Dodt and Ziegglänsberger, 1994).

Whole-cell recordings

Whole-cell recordings were performed at room temperature (~24°C; RT) following the methods described by Hamill *et al.* (1981). Electrodes with tip resistances between 2.5-3.5 MΩ were fashioned from borosilicate glass (inner diameter 0.86 mm, outer diameter 1.5 mm, GB150-8P, Science Products, Hofheim, Germany) with a temperature-controlled pipette

puller (PIP5, HEKA-Elektronik, Lambrecht, Germany). If not stated otherwise, the recording pipettes were filled with intracellular saline solution containing (in mM): 190 K-aspartate, 10 NaCl, 1 CaCl₂, 2 MgCl₂, 10 HEPES, 10 EDTA or EGTA, and adjusted to pH 7.2 with KOH, resulting in an osmolarity of ~415 mOsm and the cells were superfused constantly with extracellular saline solution containing (in mM): 185 NaCl, 4 KCl, 2 CaCl₂, 2 MgCl₂, 10 HEPES, 35 D-glucose. The solution was adjusted to pH 7.2 with NaOH and to 430 mOsm with glucose.

In the experiments in which it was crucial to quantitatively clamp the free intracellular Ca²⁺ to different levels, the solutions were made up with calculated Ca²⁺/Ca²⁺ chelator ratios to reach the desired concentration range, while Ca²⁺ influx via voltage gated Ca²⁺ channels was blocked by CdCl₂ (5 x 10⁻⁴ M). In these experiments the stated free intracellular Ca²⁺ concentrations are measured using a Ca²⁺ electrode. The calibration of the Ca²⁺ electrode was performed as described in Kay et al. 2008.

Whole-cell voltage- and current clamp recordings were made with an EPC9 patch clamp amplifier (HEKA-Elektronik) that was controlled by the program Patch Master (version 2.52, HEKA-Elektronik) running under Windows. The electrophysiological data were sampled at 20 kHz and low pass filtered at 2 kHz with a 4-pole Bessel-Filter. Compensation of the offset potential and capacitive currents was performed using the 'automatic mode' of the EPC9 amplifier. Whole-cell capacitance was determined by using the capacitance compensation (C-slow) of the amplifier. The liquid junction potential between intracellular and extracellular solution of 15.6 mV was calculated with Patcher's-Power-Tools plug-in (<http://www3.mpibpc.mpg.de/groups/neher/index.php?page=aboutppt>) for Igor Pro (Wavemetrics, Portland, Oregon) and was also compensated. To remove uncompensated leakage and capacitive currents, a p/6 protocol was used (Armstrong and Bezanilla 1974). Voltage errors due to series resistance (*R_S*) were minimized using the *R_S*-compensation of the EPC9. *R_S* was compensated between 50% and 90% with a time constant (τ) of 100 μ s. To reduce synaptic input during the current clamp recordings, 10 μ M CNQX (6-cyano-7-nitroquinoxaline-2,3-dione, C127, Sigma-Aldrich), 50 μ M DL-AP5 (DL-2-amino-5-

phosphonopentanoic acid, BN0086, Biotrend), 100 μ M PTX (picrotoxin, P1675, Sigma Aldrich), 5 μ M CGP-54626 hydrochloride (BN0597, Biotrend), and 100 μ M mecamylamine hydrochloride (M9020, Sigma-Aldrich) or 50 μ M tubocurarine (93750, Sigma Aldrich)) was added to the extracellular saline. These chemicals block glutamate-, GABA_A-, GABA_B-, and nicotinic acetylcholine receptors, respectively. Initially we used tubocurarine to block nicotinic synaptic transmission. To avoid potential interactions with SK channels it was replaced by mecamylamine, which has been shown to block nicotinic transmission in the antennal lobe of *P. americana* (Warren and Kloppenburg 2014).

The protocols for each set of the voltage clamp experiments are given in RESULTS. Current density was calculated as the ratio between current and whole-cell capacitance. To analyze changes in electrophysiological properties during the occlusion experiments, series of hyperpolarizing and depolarizing current pulses (500 ms) were applied under current clamp from a membrane potential of -60 mV. Cell input resistance was determined with series of small hyperpolarizing current pulses (20 pA - 80 pA; 20 pA increments) and the action potential waveform was analyzed during depolarizing current pulses (30 pA – 210 pA; 30 pA increments). Action potential related parameters were compared from selected spike trains, which had similar instantaneous frequencies (16Hz - 18Hz) before and during blocker application. Blocker effects on excitability (latency to first spike and number of spikes) were analyzed during current pulses (with the same amplitude before and during blocker application) with a 'control latency' of at least 100 ms.

Current isolation

$I_{K(Ca)}$ was isolated using a combination of pharmacological blockers, appropriate holding potential, and digital current subtraction protocols, based on protocols that have been effective in insect preparations (Heidel and Pflüger 2006; Husch et al. 2009; Kloppenburg and Hörner 1998; Kloppenburg et al. 1999b; Lee et al. 2014; Mercer et al. 1995, 1996; Pym et al. 2006; Ryglewski and Duch 2009; Schäfer et al. 1994). Voltage-activated transient Na⁺

currents were blocked by tetrodotoxin (10^{-6} M, TTX, T-550, Alomone, Jerusalem, Israel). The transient K^{+} current (I_A) was blocked with 4-aminopyridine (4×10^{-3} M, 4-AP, A78403, Sigma-Aldrich). Ca^{2+} currents were blocked by $CdCl_2$ (5×10^{-4} M). $I_{K(Ca)}$ could be eliminated indirectly by blocking the Ca^{2+} currents by $CdCl_2$. To compensate for changes in osmolarity, the glucose concentration was appropriately adjusted. Details of recording solutions and voltage protocols for each set of experiments are given in the Results.

Recordings from dopaminergic neurons of the mouse substantia nigra

All animal procedures were conducted in compliance with protocols approved by local government authorities (Bezirksregierung Köln, Cologne, Germany) and were in accordance with National Institutes of Health guidelines. Experiments were performed on brain slices from 12 weeks old female and male C57/Bl6 mice. Dopaminergic neurons of the substantia nigra were recorded in the whole-cell configuration following previously described experimental procedures (Hess et al. 2013; Könnner et al. 2011). The extracellular saline contained (in mM): 125 NaCl, 2.5 KCl, 1.2 NaH_2PO_4 , 10 HEPES, 2 $MgCl_2$, 5 glucose, 21 $NaHCO_3$, 2 $CaCl_2$, adjusted to pH 7.2 with NaOH resulting in an osmolarity of ~310 mOsm. The patch pipettes were filled with (in mM): 128 K-D-gluconat, 10 KCl, 10 HEPES, 2 $MgCl_2$, 0.1 EGTA, 3 ATP, 0.3 GTP, adjusted to pH 7.3 with KOH resulting in an osmolarity of ~300 mOsm.

Data analysis

Calculated values are given as mean \pm standard deviation. For IC_{50} values the 95% confidence intervals are presented in parentheses. When comparing significance between two groups of data a paired two-tailed t test was used, when comparing three groups of data ANOVA was used with a Tukey's *post-hoc* test. A significance level of 0.05 was accepted for all tests. Statistical significance is represented by one, two, or three asterisks displayed between groups of data in the figures, which represent a p -value ≤ 0.05 , ≤ 0.01 , and ≤ 0.001 ,

respectively. We used the software Igor Pro 6.0.1 (Wavemetrics, including the Patcher's PowerTools plug-in) for analysis of electrophysiological data and GraphPad Prism 5 (GraphPad Software, San Diego, CA) for statistical analysis.

Single cell labeling

To label individual cells, 1% (w/v) biocytin (B4261, Sigma-Aldrich, Taufkirchen, Germany) was added to the pipette solution. After the electrophysiological recordings, the brains were fixed in Roti-Histofix (2-3 h, TR; P0873, Carl Roth, Karlsruhe, Germany) at room temperature (RT). Subsequently the brains were rinsed in phosphate buffered saline (PBS, 3 x 20 min, RT). All brains were processed as whole-mounts. To facilitate the streptavidin penetration, the brains were treated with a commercially available collagenase/dispase mixture (1 mg · ml⁻¹, 269638, Roche Diagnostics, Mannheim, Germany) and hyaluronidase (1 mg · ml⁻¹, H3506, Sigma-Aldrich, Taufkirchen, Germany) in PBS (20 min, 37°C), rinsed in PBS (3 x 10 min, 4°C), incubated in PBS containing 1% (w/v) Triton X-100 (A1388, Applichem, Darmstadt, Germany) and 10% normal goat serum (40 min, RT, S-1000, Linaris, Wertheim, Germany) and rinsed again in PBS (3 x 10 min, 4°C). Afterwards, the brains were incubated in Alexa Fluor 633 (Alexa 633) conjugated streptavidin (1:400, 1-2 days, 4°C, S21375, Life technologies, Darmstadt, Germany) that was dissolved in PBS containing 10% (v/v) normal goat serum. Brains were rinsed in PBS (3 x 10 min, 4°C), dehydrated, and cleared and mounted in methylsalicylate (M6752, Sigma-Aldrich, Taufkirchen, Germany).

The fluorescence images were captured with a confocal microscope (LSM 510, Carl Zeiss, Göttingen, Germany) equipped with Plan-Neofluar 10x (0.3 NA), Plan-Apochromat 20x (0.75 NA), and Plan-Apochromat 63x (1.4 NA Oil) objectives. Streptavidin-Alexa 633 was excited with a He-Ne Laser at 633 nm. Emission of Alexa 633 was collected through a 650 nm long-pass filter. Scaling, contrast and brightness adjustment, and z-projections were performed with ImageJ (version 1.47v) and the WCIF plugin bundle (www.uhnresearch.ca/facilities/wcif/). For overview images overlapping image stacks were

merged in Photoshop CS5 (Adobe Systems Incorporated, San Jose, CA). The final figures were prepared with Photoshop CS5 and Illustrator CS5 (Adobe Systems).

RESULTS

In most neurons Ca^{2+} dependent K^+ currents are crucial in shaping their intrinsic firing properties. Here we aimed to characterize $I_{\text{K}(\text{Ca})}$ in uPNs, which are key components of the insect olfactory system. The study was performed in two steps. First we characterized the functional properties of $I_{\text{K}(\text{Ca})}$ in uPNs with whole-cell voltage clamp recordings in an intact brain preparation of male *P. americana*. Second, we used occlusion experiments, in which portions of $I_{\text{K}(\text{Ca})}$ were pharmacologically blocked, to better understand the functional role of $I_{\text{K}(\text{Ca})}$ in shaping the electrophysiological properties of uPNs.

The recordings were performed under visual control from cell bodies in the ventral portion of the ventrolateral somata group (VSG) (Distler 1990; Fusca et al. 2013, 2015; Husch et al. 2009) in an intact brain preparation. These somata belong mostly to a relatively homogeneous population of uPNs. During the recordings the neurons were labelled with biocytin/streptavidin to confirm the identity of the recorded neurons. Each of the recorded uPNs had arborizations in a single glomerulus and sent its axon through the medial antennal lobe tract (mALT) to the protocerebrum (Malun et al. 1993; Nishino et al. 2003, 2010; Watanabe et al. 2010, 2012), innervating the mushroom body calyces and the lateral horn (Fig. 1 A1-A4). Since we did not find any systematic differences in the electrophysiological properties that would justify a separation into distinct uPN classes, we pooled the data for the analysis. It has yet to be shown if other PN types have similar properties.

Isolation of $I_{\text{K}(\text{Ca})}$.

$I_{\text{K}(\text{Ca})}$ was isolated using a combination of pharmacological tools, appropriate holding potentials, and current subtraction protocols (Fig. 1 B-E). The preparation was superfused with saline containing 10^{-6} M TTX and 4×10^{-3} 4-AP. If not stated otherwise the Ca^{2+}

concentration during the voltage clamp experiments was 1 mM and the neurons were held at -60 mV between voltage protocols. As a result of these current isolation protocols the current profiles were clearly dominated by $I_{K(Ca)}$, but they may still have included small residuals of other currents. The current waveforms did not indicate significant voltage control problems (e.g. no delay of current onset, no jumps in the voltage-dependence), suggesting that they originated mostly from well voltage-clamped regions. Given the long, thin primary neurite, we assume that a major portion or all of the currents we measured originated from the cell bodies.

To determine the current-voltage (I - V) relation, two series of 300 ms voltage pulses were delivered in 10 mV increments between -60 and +60 mV (Fig. 1 B). During the second series the extracellular saline additionally contained 5×10^{-4} M $CdCl_2$ (Fig. 1 C), which completely abolished voltage-activated Ca^{2+} currents (Husch et al. 2008). Accordingly, under Cd^{2+} the peak current was drastically reduced and the inverted U-shape of the I - V relation was eliminated. The difference between the 'untreated' and the ' Cd^{2+} -treated' current series was defined as $I_{K(Ca)}$ (Fig. 1 D). When defined like this, $I_{K(Ca)}$ contains I_{Ca} . Since the inward I_{Ca} is very small compared to the whole current ($\sim 5\%$; Fig. 7) it does not affect the conclusions of the experiments. $I_{K(Ca)}$ activated with voltage steps more depolarized than -40 mV and consisted of a fast and slowly decaying component. This decay kinetics during a sustained voltage pulse reflected the inactivation of I_{Ca} (Husch et al. 2009). $I_{K(Ca)}$ had a pronounced inverted U-shaped I - V relation (Fig. 1 E; Fig. 2 A-C) which mirrored the I - V relation of I_{Ca} (Husch et al. 2009). On average the maximal peak current was 21.3 ± 6.1 nA ($n=7$). Given a mean whole-cell capacitance of 17.9 ± 3.7 pF, this corresponded to a mean current density of 1.23 ± 0.46 nA \cdot pF $^{-1}$. On average the maximal peak current was reached at 17 ± 11 mV ($n=7$) and decreased at more depolarized voltage steps as the driving force for Ca^{2+} declined. Note that these values differed from the maxima of the mean I - V and of the *current density*- V plots, since the membrane potential at which the maximal currents occurred varied between cells (Fig. 2 A-C). Assuming that the main charge carrier is K^+ this corresponds to a conductance density of 11 ± 4.7 nS \cdot pF $^{-1}$ (110 ± 47 pS \cdot μm^{-2}). Increasing the extracellular

Ca²⁺ concentration from 1 mM to 6 mM altered the *I*-*V* relation from an inverted U-shaped to a more linearly increasing *I*-*V* relation (Fig. 2 D).

Calcium dependence of $I_{K(Ca)}$.

Our first series of experiments demonstrated that $I_{K(Ca)}$ is voltage and Ca²⁺ dependent. However, the exact time course and amplitude of this outward current are complex functions of membrane potential, intracellular Ca²⁺ concentration at the K_{Ca} channel, voltage and Ca²⁺ dependence of I_{Ca} , and the Ca²⁺ dependence of the underlying K_{Ca} channels. Accordingly, only limited conclusions about the intrinsic activation and inactivation properties can be made from the shape of whole-cell currents activated by simple depolarizing voltage steps. To further study the Ca²⁺ dependence of $I_{K(Ca)}$ we used two-step voltage protocols (Solaro et al. 1995). A test pulse depolarized the membrane to +60 mV, where virtually no voltage activated Ca²⁺ influx occurs, since the membrane voltage approaches the Ca²⁺ equilibrium potential. The +60 mV test pulse was preceded by depolarizing voltage pulses (Ca²⁺ loading-steps) of varying amplitude (Fig. 3 A) or duration (Fig. 3 B) which modified the Ca²⁺ influx and thereby the intracellular Ca²⁺ concentration in the vicinity of the K_{Ca} channel. Thus, during the +60 mV test pulse, $I_{K(Ca)}$ was activated a) by the strongly depolarized membrane potential and b) by the Ca²⁺ resting level plus the varying amount of Ca²⁺ delivered by I_{Ca} during the loading-pulse. Taking into account that I_{Ca} inactivates during a sustained voltage pulse, the instantaneous Ca²⁺ influx during the loading-pulse depended a) on the potential of the loading-pulse and b) on the duration of I_{Ca} activation.

In a first set of experiments we used 200 ms loading-steps from -60 mV to +60 mV with 10 mV increments. This voltage range covered the complete voltage operating range of I_{Ca} in uPNs (Husch et al. 2009). During the loading-steps $I_{K(Ca)}$ was activated (Fig. 3 A,B) as shown already in Fig. 1. Figure 3 A1 shows the current in response to a +60 mV test pulse that was preceded by loading-pulses to +10 mV (large Ca²⁺ influx) and to +60 mV (virtually no Ca²⁺ influx) (compare with Fig. 2 A-C). The Ca²⁺ influx that is induced by the +10 mV pulse is terminated at the start of the +60 mV test pulse. Accordingly, during the +60 mV test

pulse $I_{K(Ca)}$ was activated by the depolarized membrane potential and the residual Ca^{2+} from the +10 mV loading-pulse. Thus, $I_{K(Ca)}$ that was activated during the test pulse is transient with fast deactivation (Fig. 3 A1), whereby the time course of the deactivation is strongly dependent on the decaying residual intracellular Ca^{2+} concentration. The whole experiment with the complete set of loading-pulses is shown in Figure 3 A2-A3. Plotting the transient peak $I_{K(Ca)}$ during the test pulses over the potentials of the loading-pulses (Fig. 3 A4) revealed inverted U-shaped relations with an average maximum of 11.7 ± 13.3 mV ($n = 6$), which is within the voltage range where I_{Ca} has its maximum (Husch et al. 2009). The mirrored I - V relations of I_{Ca} and $I_{K(Ca)}$ clearly demonstrated the strong Ca^{2+} dependence of $I_{K(Ca)}$.

In a second set of experiments the +60 mV test pulse was preceded by loading-steps with increasing duration from 5 ms to 400 ms (Fig. 3 B). For each experiment the loading-step voltage was set to the value at which we observed the maximal current during the +60 mV test pulse in the first part of the experiment (previous paragraph). Due to the inactivation of I_{Ca} during a sustained depolarization (Husch et al. 2009) the instantaneous Ca^{2+} influx at the end of each loading-pulse was decreasing with increasing duration of the loading-pulses. Therefore, the amplitude of the transient peak $I_{K(Ca)}$ during the +60 mV test pulses decreased with increasing loading-pulse duration (Fig. 3 B1-B2), again demonstrating the strong Ca^{2+} dependence of $I_{K(Ca)}$.

Voltage dependence of $I_{K(Ca)}$

Next we studied the steady state voltage dependence, the voltage inactivation during a sustained depolarization, and the Ca^{2+} dependence directly and independently of each other. A series of voltage pulses was applied in 10 mV increments between -60 mV and +60 mV, while the cytosolic Ca^{2+} concentration was clamped at different concentrations using an EDTA or EGTA - Ca^{2+} buffering system and by blocking I_{Ca} with 5×10^{-4} M $CdCl_2$. The concentration of free cytosolic Ca^{2+} $[Ca^{2+}]_i$ was clamped at 56 μ M, 143 μ M, mM, 540 μ M, or 1800 μ M. These values were measured using a Ca^{2+} electrode. Under clamped $[Ca^{2+}]_i$ $I_{K(Ca)}$ did not inactivate during a sustained voltage pulse (Fig. 4 A,B), showing directly that the

decay of $I_{K(Ca)}$ as shown in Figure 1 depends on the I_{Ca} kinetics. At all cytosolic Ca^{2+} concentrations $I_{K(Ca)}$ increased with increasing depolarization showing a clear voltage dependence for steady state activation (Fig. 4). Comparing conductance-voltage (G-V) relations for the different $[Ca^{2+}]_i$ showed that increasing Ca^{2+} concentrations lowered the voltage threshold for activation of $I_{K(Ca)}$ and the voltage for half-maximal activation ($V_{0.5,act}$) (Fig 4 C,D). For example: $V_{0.5,act}$ was 125 ± 12 mV ($n = 5$) at $[Ca^{2+}]_i = 56 \mu M$ and 50 ± 14 mV ($n = 6$) at $[Ca^{2+}]_i = 1800 \mu M$ ($p < 0.02$; unpaired test). We did not observe a ' Ca^{2+} block' at high $[Ca^{2+}]_i$.

Effects of apamin, charybdotoxin and iberiotoxin on $I_{K(Ca)}$.

In principle depolarizing voltage steps with the resulting Ca^{2+} influx can activate both SK and BK channels. Here we tested the effect of apamin, charybdotoxin (CTX) and iberiotoxin (IbTX) on $I_{K(Ca)}$, which are toxins that have been shown to block specific components of $I_{K(Ca)}$ in vertebrates (Bennett et al. 2000; Blatz and Magleby 1986; Faber and Sah 2003; Fioretti et al. 2004; Galvez et al. 1990; Ghatta et al. 2006; Giangiacomo et al. 1992; Kaczorowski et al. 1996; Pineda et al. 1992; Wolfart et al. 2001). Apamin blocks SK (K_{Ca} 2.1, K_{Ca} 2.2, K_{Ca} 2.3) channels and iberiotoxin blocks BK (K_{Ca} 1.1) channels. Charybdotoxin not only blocks BK (K_{Ca} 1.1) channels but has also been shown to block IK (K_{Ca} 3.1) and K_V (K_V 1.2; K_V 1.3) channels. Ideally such blockers could be used a) for occlusion experiments during current clamp recordings to analyze the role of $I_{K(Ca)}$ in shaping the intrinsic firing properties of uPNs and b) to get information about the molecular identity of the channels that mediate $I_{K(Ca)}$ in uPNs.

Both ChTX and IbTX reduced $I_{K(Ca)}$ in a concentration dependent way (Fig. 5 A,B) while apamin had no effect (data not shown). The concentration-response relations were determined with concentrations ranging from 50 pM to 100 nM and were well fit with the sigmoidal relation

$$F(x) = Bottom + \frac{(Top - Bottom)}{(1 + 10^{(x - x_{50})})} \quad (1)$$

(Fig. 5 B). CTX started to block $I_{K(Ca)}$ at concentrations higher than ~100 pM and completely abolished $I_{K(Ca)}$ at concentrations higher than ~30 nM. The concentration response relation had an IC_{50} of 2.7 nM (1.8 nM – 3.8 nM). IbTX started to block $I_{K(Ca)}$ at concentrations around 100 pM and blocked maximally ~60% of $I_{K(Ca)}$ at concentrations of ~10 nM and higher. The concentration response relation had an IC_{50} of 157 pM (53.7 pM to 460 pM). Apamin was applied in concentrations up to 1 μ M with no detectable effect on $I_{K(Ca)}$. Since previous work had shown that I_{SK} in insect neurons can be insensitive to apamin (Abou Tayoun et al. 2011; Wicher et al. 2001), we used voltage clamp protocols, which have been used to evoke I_{SK} in rodents (Chen et al. 2014; Wolfart et al. 2001), to probe for SK channels in uPNs. In these experiments neurons were held at -60 mV. To elicit I_{SK} a 100 ms depolarizing voltage pulse (Ca^{2+} loading-pulse) to 0 mV was applied, that was preceded by a 1 s hyperpolarizing pulse to -80 mV. In dopaminergic substantia nigra neurons of mice this protocol evoked an apamin (100 nM) sensitive I_{SK} (Fig. 6 A). Using the same protocol, we did not detect I_{SK} in uPNs (Fig. 6 B). To ensure the 'right parameter space' of the loading-pulse, its amplitude (-40 mV to +50 mV) and duration (10 ms to 200 ms) were varied.

Since CTX (100 nM) completely blocked $I_{K(Ca)}$, we compared the residual currents after the direct CTX block of $I_{K(Ca)}$ with the residual currents after the indirect block of $I_{K(Ca)}$ using Cd^{2+} (Fig. 7). As expected, in contrast to the Cd^{2+} block, the residual current after CTX block still contained I_{Ca} (Fig. 7E).

The role of $I_{K(Ca)}$ on spike waveform

Clearly odor responses and tuning profiles of uPNs are determined by their synaptic input and by their intrinsic electrophysiological properties. In synaptically isolated uPNs depolarizing current injections induced trains of action potentials with fairly regular firing patterns. Typically, the spike frequency increased during a prolonged depolarization. We did not observe spike frequency adaptation. To better understand the role of $I_{K(Ca)}$ in mediating the intrinsic electrophysiological properties we performed occlusion experiments under

current clamp in which $I_{K(Ca)}$ was partially blocked by the $I_{K(Ca)}$ blockers CTX or IbTX. In synaptically connected neurons application of 100 nM CTX, which blocked 100% of $I_{K(Ca)}$, resulted in an unstable membrane potential and spontaneous high frequency bursts of action potentials (data not shown). These drastic effects of completely blocking $I_{K(Ca)}$ indicated the important role of $I_{K(Ca)}$ in shaping the intrinsic electrophysiological and synaptic properties of AL neurons. Based on these experiments the blocker concentration was reduced to block maximally 60% to 80% of $I_{K(Ca)}$, and we also blocked synaptic input pharmacologically (see METHODS). Before, during and after the application of the $I_{K(Ca)}$ blockers, we applied current injection protocols to analyze a set of intrinsic electrophysiological properties. These included resting membrane potential, cell input resistance, action potential repolarization rate, action potential width, action potential afterhyperpolarization, latency to the first action potential upon depolarizing current injection, firing threshold, and number of elicited action potentials. Details of the current clamp protocols are given in METHODS.

Charybdotoxin. 10 nM CTX, which blocked ~80% of $I_{K(Ca)}$ (Fig. 5), changed the action potential waveform significantly (Fig. 8; Fig. 9A). The maximal rate of action potential repolarization was reduced from -174 ± 16 to -119 ± 10 mV \cdot s $^{-1}$ ($p < 0.001$; $n = 10$; Fig. 9 A1). Accordingly, the spike width at half-maximal amplitude was increased from 505 ± 60 μ s to 668 ± 40 μ s ($p < 0.001$; $n = 10$; Fig. 9 A2) and the action potential afterhyperpolarization was reduced ($p < 0.001$; $n = 10$; Fig. 9 A3). During constant 500 ms depolarizing current pulses, the latency to the first spike decreased from 252 ± 106 ms to 123 ± 46.8 ms ($p < 0.01$; $n = 10$; Fig. 9 A4) and the number of spikes increased from 6 ± 3 to 13.3 ± 2.8 ($p < 0.001$; $n = 10$; Fig. 9 A6). The threshold for spike initiation (Fig. 9 A5), the resting membrane potential and cell input resistance (measured around the resting membrane potential) did not change (data not shown). All of the observed CTX effects were at least in part reversible.

Iberiotoxin. IbTX was applied at concentrations of 100 nM IbTX, where it had its maximal effect and blocked ~60% of $I_{K(Ca)}$ (Fig. 5). Generally, 100 nM IbTX had similar but weaker effects than 10 nM CTX. IbTX decreased the repolarization rate from $194 \pm 26 \text{ V} \cdot \text{s}^{-1}$ to $130 \pm 34 \text{ V} \cdot \text{s}^{-1}$ ($p < 0.001$; $n = 11$; Fig. 9 B1), increased spike width from $430 \pm 49 \mu\text{s}$ to $561 \pm 125 \mu\text{s}$ ($p < 0.001$, $n = 11$; Fig. 9 B2), and reduced the action potential afterhyperpolarization ($p < 0.001$; $n = 11$; Fig. 9 B3). The latency to the first spike decreased from $146 \pm 20 \text{ ms}$ to $95 \pm 53 \text{ ms}$ ($p < 0.05$; $n = 7$; Fig. 9 B4) and the number of spikes increased from 6.5 ± 1.5 to 9.6 ± 2 ($p < 0.05$; $n = 7$; Fig. 9 B6). All these effects were reversible upon wash out. IbTX had no significant effects on firing threshold (Fig. 9 B5), cell input resistance (measured around the resting membrane potential), and resting membrane potential (data not shown).

Apamin. In agreement with our voltage clamp experiments, in which apamin had no effect on $I_{K(Ca)}$ and in which we did not detect I_{SK} (Fig. 6), there was no effect of $1 \mu\text{M}$ apamin on the membrane potential or spike related properties (Fig. 9C).

DISCUSSION

The overall goal of this study was to characterize $I_{K(Ca)}$ in uPNs. In the insect brain uPNs form the principal pathway from the AL to the protocerebrum, where centers for multimodal sensory processing and learning, and relays for innate behaviors are located (Davis 2004; Heimbeck et al. 2001; Heisenberg 2003; Stopfer 2014). Ca^{2+} -activated currents are an important link between the intracellular signaling system and the membrane potential of the cell. In most neuron types $I_{K(Ca)}$ is pivotal for shaping intrinsic electrophysiological properties. Accordingly, we performed the study in two steps. First, we characterized the functional properties of $I_{K(Ca)}$. Second, we used occlusion experiments, in which portions of $I_{K(Ca)}$ were pharmacologically blocked, to reveal the role of $I_{K(Ca)}$ in shaping the intrinsic electrophysiological properties of uPNs. For all recordings we used the whole-cell patch

clamp configuration combined with single cell labeling in an intact, adult brain preparation of *P. americana*.

In general, $I_{K(Ca)}$ in uPNs was similar to Ca^{2+} -activated K^+ currents found in other insect neurons (Derst et al. 2003; Grolleau and Lapied 1996; Grünewald 2003; Heidel and Pflüger 2006; Kulke et al. 2014; Lucas and Shimahara 2002; Perk and Mercer 2006; Pézier et al. 2007; Ryglewski and Duch 2009; Schäfer et al. 1994). $I_{K(Ca)}$ had the typical inverted U-shaped I - V relation and $I_{K(Ca)}$ decayed during a sustained depolarizing voltage pulse, but did not inactivate when $[Ca^{2+}]_i$ was clamped to constant values. The strong Ca^{2+} dependence of $I_{K(Ca)}$ is corroborated by the inverted U-shaped I - V relation that mirrored the I - V relation of I_{Ca} and also the decay kinetics during a sustained voltage pulse, which reflected the inactivation kinetics of I_{Ca} (Husch et al. 2009). The Ca^{2+} dependence is also shown in the loading-pulse experiments where $I_{K(Ca)}$ activated transiently with a very fast decay during the +60 mV test pulse (where virtually no Ca^{2+} is entering the cell). The transient activation and fast decay of $I_{K(Ca)}$ in these experiments indicated a close spatial relation of the Ca^{2+} and K_{Ca} channels (Augustine et al. 2003; Berkefeld et al. 2010) and efficient Ca^{2+} sequestration (Pippow et al. 2009) leading to a fast attenuation of the Ca^{2+} microdomain in the vicinity of the K_{Ca} channel. Taken together our data demonstrate that $I_{K(Ca)}$ is directly linked to the voltage-activated Ca^{2+} influx and that it is strongly Ca^{2+} and voltage dependent. Following the classical biophysical classification of K_{Ca} channels our results suggest that $I_{K(Ca)}$ in uPNs is mediated by BK channels, since it required depolarized membrane potential and elevated intracellular Ca^{2+} . This notion is in line with our pharmacological experiments. We found sensitivity of $I_{K(Ca)}$ to IbTX and CTX, but not to apamin. However, these experiments have to be interpreted with caution. IbTX, which is considered a specific BK (K_{Ca} 1.1) channel blocker, reduced $I_{K(Ca)}$ by 60%, while the less specific blocker CTX completely abolished $I_{K(Ca)}$. CTX not only blocks BK (K_{Ca} 1.1) channels but has also been shown to block IK (K_{Ca} 3.1) and K_V (K_V 1.2; K_V 1.3) channels (Garcia et al. 1995). Accordingly, this might indicate that IK channels also contribute to $I_{K(Ca)}$. Given that our current isolation protocol selected for true Ca^{2+} dependent currents, K_V channels did not contribute to the current that we define as $I_{K(Ca)}$. Our results are

also in line with previous work from Derst et al. (2003) who cloned pSlo, the BK channel α subunit of *P. americana*, and expressed it in HEK 293 cells. The resulting whole-cell current had similar properties as $I_{K(Ca)}$ in uPNs. It had a clear Ca^{2+} and voltage dependence, and did not inactivate under clamped $[Ca^{2+}]_i$.

Apamin, which is considered a specific SK channel (K_{Ca} 2.1, K_{Ca} 2.2, K_{Ca} 2.3) blocker (Adelman et al. 2012), had no effect on $I_{K(Ca)}$. Since previous work has shown that SK channels in insects can be insensitive to apamin (Abou Tayoun et al. 2011; Wicher et al. 2001), we used voltage clamp protocols that induce I_{SK} in dopaminergic midbrain neurons of mice. These experiments did not reveal I_{SK} in uPNs and suggest that uPNs of *P. americana* do not express SK channels. While these results seem somewhat unexpected, they are in agreement with in situ hybridization experiments which suggest that SK channels are indeed not expressed in AL neurons of *P. americana* (S. Korsching, V. Zapilko and D. Fusca, personal communication). A straightforward and tempting conclusion is that the lack of I_{SK} makes the resting membrane potential of uPNs relatively independent of the resting $[Ca^{2+}]_i$, since I_{BK} requires high $[Ca^{2+}]_i$ and a depolarized membrane potential.

The occlusion experiments with high concentrations of CTX, which completely blocked $I_{K(Ca)}$ (I_{BK}), increased synaptic input and excitability of uPNs indicated the significant physiological role of $I_{K(Ca)}$ in neurons of the AL network. To reveal in more detail how $I_{K(Ca)}$ contributes to shaping the intrinsic electrophysiological properties of uPNs, we performed experiments on synaptically isolated uPNs in which $I_{K(Ca)}$ was only moderately blocked. A 60% to 80% block of $I_{K(Ca)}$ (I_{BK}) significantly changed the action potential waveform and excitability, which is in agreement with the roles of $I_{K(Ca)}$ that have been observed in other neuron types of different species (Berkefeld et al. 2010; Faber and Sah 2003; Greffrath et al. 2004; Kadas et al. 2015). By linking free $[Ca^{2+}]_i$ and membrane potential BK channels contribute to regulating the intrinsic electrophysiological properties. BK channels are rapidly activated during the rising phase of the action potential by the depolarizing membrane potential and the voltage dependent Ca^{2+} influx. Once activated, BK channels influence the rate of action potential repolarization and action potential afterhyperpolarization (Berkefeld et

al. 2010; Faber and Sah 2003; Greffrath et al. 2004), thus they directly contribute to the control of action potential waveform and spike frequency (Berkefeld et al. 2010; Faber and Sah 2003; Greffrath et al. 2004; Kadas et al. 2015).

All the recordings in this study were performed in an intact brain preparation, in which the currents are not altered by any culturing procedure or in vitro development. Given that the complex arborizations are still intact, perfect voltage control across the whole neuron is impossible. The current waveforms usually did not indicate significant voltage control problems (e.g. no delay of current onset, no jumps in the I - V relation) suggesting that they originated mostly from well voltage-clamped regions. Since we recorded from the soma, which has a long thin neurite connecting it to the rest of the cell, it is likely that the currents we have measured originate primarily from the cell body. Ionic currents generated by channels selectively located in very distal regions of the neuron may not be detectable by voltage-clamping the soma.

Because intrinsic electrophysiological properties of neurons are determined by the expressed ion channel types and by their expression ratio, we consider such a detailed analysis of the biophysical properties an important prerequisite to conductance-based models to gain a clear understanding of how olfactory signals are processed at the single cell and circuit level.

Acknowledgements

We thank Helmut Wratil for excellent technical assistance.

Grants

This work was supported by grant KL 762/5-1 from the Deutsche Forschungsgemeinschaft, a CONNECT grant, and a Max-Delbrück Award from the UoC to PK, and an Alexander von Humboldt fellowship awarded to BW.

REFERENCES

- Abou Tayoun AN, Li X, Chu B, Hardie RC, Juusola M, Dolph PJ.** The Drosophila SK channel (dSK) contributes to photoreceptor performance by mediating sensitivity control at the first visual network. *J Neurosci* 31: 13897–13910, 2011.
- Adelman JP, Maylie J, Sah P.** Small-Conductance Ca^{2+} -Activated K^{+} Channels: Form and Function. *Annu Rev Physiol* 74: 245–269, 2012.
- Armstrong CM, Bezanilla F.** Charge Movement Associated with the Opening and Closing of the Activation Gates of the Na Channels. *J Gen Physiol* 63: 533–552, 1974.
- Augustine GJ, Santamaria F, Tanaka K.** Local calcium signaling in neurons. *Neuron* 40: 331–346, 2003.
- Bargmann CI.** Chemosensation in *C. elegans*. *WormBook Online Rev. C Elegans Biol.* (2006). doi: 10.1895/wormbook.1.123.1.
- Bennett BD, Callaway JC, Wilson CJ.** Intrinsic membrane properties underlying spontaneous tonic firing in neostriatal cholinergic interneurons. *J Neurosci* 20: 8493–8503, 2000.
- Berkefeld H, Fakler B, Schulte U.** Ca^{2+} -activated K^{+} channels: from protein complexes to function. *Physiol Rev* 90: 1437–1459, 2010.
- Blatz AL, Magleby KL.** Single apamin-blocked Ca^{2+} -activated K^{+} channels of small conductance in cultured rat skeletal muscle. *Nature* 323: 718–720, 1986.
- Broome BM, Jayaraman V, Laurent G.** Encoding and Decoding of Overlapping Odor Sequences. *Neuron* 51: 467–482, 2006.
- Chen S, Benninger F, Yaari Y.** Role of Small Conductance Ca^{2+} -Activated K^{+} Channels in Controlling CA1 Pyramidal Cell Excitability. *J Neurosci* 34: 8219–8230, 2014.
- Christensen TA, Waldrop BR, Hildebrand JG.** Multitasking in the Olfactory System: Context-Dependent Responses to Odors Reveal Dual GABA-Regulated Coding Mechanisms in Single Olfactory Projection Neurons. *J Neurosci* 18: 5999–6008, 1998.
- Davis RL.** Olfactory learning. *Neuron* 44: 31–48, 2004.
- Derst C, Messutat S, Walther C, Eckert M, Heinemann SH, Wicher D.** The large conductance Ca^{2+} -activated potassium channel (pSlo) of the cockroach *Periplaneta americana*: structure, localization in neurons and electrophysiology. *Eur J Neurosci* 17: 1197–1212, 2003.
- Distler P.** Synaptic connections of dopamine-immunoreactive neurons in the antennal lobes of *Periplaneta americana*. Colocalization with GABA-like immunoreactivity. *Histochemistry* 93: 401–408, 1990.
- Faber ESL, Sah P.** Physiological Role of Calcium-Activated Potassium Currents in the Rat Lateral Amygdala. *J Neurosci* 22: 1618–1628, 2002.
- Faber ESL, Sah P.** Calcium-Activated Potassium Channels: Multiple Contributions to Neuronal Function. *The Neuroscientist* 9: 181–194, 2003.

586 **Fakler B, Adelman JP.** Control of K_{Ca} Channels by Calcium Nano/Microdomains. *Neuron*
587 59: 873–881, 2008.

588 **Fioretti B, Castigli E, Calzuola I, Harper AA, Franciolini F, Catacuzzeno L.** NPPB block
589 of the intermediate-conductance Ca^{2+} -activated K^{+} channel. *Eur J Pharmacol* 497: 1–6, 2004.

590 **Fusca D, Husch A, Baumann A, Kloppenburg P.** Choline acetyltransferase-like
591 immunoreactivity in a physiologically distinct subtype of olfactory nonspiking local
592 interneurons in the cockroach (*periplaneta americana*). *J Comp Neurol* 521: 3556–3569,
593 2013.

594 **Fusca D, Schachtner J, Kloppenburg P.** Colocalization of allatotropin and tachykinin-
595 related peptides with classical transmitters in physiologically distinct subtypes of olfactory
596 local interneurons in the cockroach (*Periplaneta americana*). *J Comp Neurol* 523:1569-1586,
597 2015.

598 **Galizia CG, Rössler W.** Parallel olfactory systems in insects: anatomy and function. *Annu*
599 *Rev Entomol* 55: 399–420, 2010.

600 **Galvez A, Gimenez-Gallego G, Reuben JP, Roy-Contancin L, Feigenbaum P,**
601 **Kaczorowski GJ, Garcia ML.** Purification and characterization of a unique, potent, peptidyl
602 probe for the high conductance calcium-activated potassium channel from venom of the
603 scorpion *Buthus tamulus*. *J Biol Chem* 265: 11083–11090, 1990.

604 **Garcia ML, Knaus HG, Munujos P, Slaughter RS, Kaczorowski GJ.** Charybdotoxin and its
605 effects on potassium channels. *Am J Physiol - Cell Physiol* 269: C1–C10, 1995.

606 **Ghatta S, Nimmagadda D, Xu X, O'Rourke ST.** Large-conductance, calcium-activated
607 potassium channels: Structural and functional implications. *Pharmacol Ther* 110: 103–116,
608 2006.

609 **Giangiacoimo KM, Garcia ML, McManus OB.** Mechanism of iberiotoxin block of the large-
610 conductance calcium-activated potassium channel from bovine aortic smooth muscle.
611 *Biochemistry (Mosc)* 31: 6719–6727, 1992.

612 **Greffrath W, Magerl W, Disque-Kaiser U, Martin E, Reuss S, Boehmer G.** Contribution of
613 Ca^{2+} -activated K^{+} channels to hyperpolarizing after-potentials and discharge pattern in rat
614 supraoptic neurones. *J Neuroendocrinol* 16: 577–588, 2004.

615 **Grolleau F, Lapied B.** Two distinct low-voltage-activated Ca^{2+} currents contribute to the
616 pacemaker mechanism in cockroach dorsal unpaired median neurons. *J Neurophysiol* 76:
617 963–976, 1996.

618 **Grünewald B.** Differential expression of voltage-sensitive K^{+} and Ca^{2+} currents in neurons of
619 the honeybee olfactory pathway. *J Exp Biol* 206: 117–129, 2003.

620 **Grunnet M, Kaufmann WA.** Coassembly of Big Conductance Ca^{2+} -activated K^{+} Channels
621 and L-type Voltage-gated Ca^{2+} Channels in Rat Brain. *J Biol Chem* 279: 36445–36453, 2004.

622 **Heidel E, Pflüger H-J.** Ion currents and spiking properties of identified subtypes of locust
623 octopaminergic dorsal unpaired median neurons. *Eur J Neurosci* 23: 1189–1206, 2006.

624 **Heimbeck G, Bugnon V, Gendre N, Keller A, Stocker RF.** A central neural circuit for
625 experience-independent olfactory and courtship behavior in *Drosophila melanogaster*. *Proc*
626 *Natl Acad Sci* 98: 15336–15341, 2001.

627 **Heisenberg M.** Mushroom body memoir: from maps to models. *Nat Rev Neurosci* 4: 266–
628 275, 2003.

629 **Hess ME, Hess S, Meyer KD, Verhagen LAW, Koch L, Brönneke HS, Dietrich MO,**
630 **Jordan SD, Saletore Y, Elemento O, Belgardt BF, Franz T, Horvath TL, Rüther U,**
631 **Jaffrey SR, Kloppenburg P, Brüning JC.** The fat mass and obesity associated gene (Fto)
632 regulates activity of the dopaminergic midbrain circuitry. *Nat Neurosci* 16: 1042–1048, 2013.

633 **Hildebrand JG, Shepherd GM.** MECHANISMS OF OLFACTORY
634 DISCRIMINATION: Converging Evidence for Common Principles Across Phyla. *Annu Rev*
635 *Neurosci* 20: 595–631, 1997.

636 **Husch A, Hess S, Kloppenburg P.** Functional parameters of voltage-activated Ca^{2+}
637 currents from olfactory interneurons in the antennal lobe of *Periplaneta americana*. *J*
638 *Neurophysiol* 99: 320–332, 2008.

639 **Husch A, Paehler M, Fusca D, Paeger L, Kloppenburg P.** Calcium current diversity in
640 physiologically different local interneuron types of the antennal lobe. *J Neurosci* 29: 716–726,
641 2009.

642 **Kaczorowski GJ, Knaus HG, Leonard RJ, McManus OB, Garcia ML.** High-conductance
643 calcium-activated potassium channels; structure, pharmacology, and function. *J Bioenerg*
644 *Biomembr* 28: 255–267, 1996.

645 **Kadas D, Ryglewski S, Duch C.** Transient BK outward current enhances motoneurone
646 firing rates during drosophila larval locomotion. *J Physiol* 593: 4871–4888, 2015.

647 **Kanzaki R, Arbas EA, Strausfeld NJ, Hildebrand JG.** Physiology and morphology of
648 projection neurons in the antennal lobe of the male moth *Manduca sexta*. *J Comp Physiol [A]*
649 165: 427–453, 1989.

650 **Kay JW, Steven RJ, McGuigan JAS, Elder HY.** Automatic determination of ligand purity
651 and apparent dissociation constant in buffer solutions and the for anion binding in
652 physiological solutions from -macroelectrode measurements. *Comput Biol Med* 38: 101–110,
653 2008.

654 **Kloppenburg, Hörner** Voltage-activated currents in identified giant interneurons isolated
655 from adult crickets *gryllus bimaculatus*. *J Exp Biol* 201: 2529–2541, 1998.

656 **Kloppenburg P, Ferns D, Mercer AR.** Serotonin enhances central olfactory neuron
657 responses to female sex pheromone in the male sphinx moth *manduca sexta*. *J Neurosci* 19:
658 8172–8181, 1999a.

659 **Kloppenburg P, Kirchhof BS, Mercer AR.** Voltage-activated currents from adult honeybee
660 (*Apis mellifera*) antennal motor neurons recorded in vitro and in situ. *J Neurophysiol* 81: 39–
661 48, 1999b.

662 **Könner AC, Hess S, Tovar S, Mesaros A, Sánchez-Lasheras C, Evers N, Verhagen**
663 **LAW, Brönneke HS, Kleinriders A, Hampel B, Kloppenburg P, Brüning JC.** Role for
664 insulin signaling in catecholaminergic neurons in control of energy homeostasis. *Cell Metab*
665 13: 720–728, 2011.

666 **Kulke D, von Samson-Himmelstjerna G, Miltsch SM, Wolstenholme AJ, Jex AR, Gasser**
667 **RB, Ballesteros C, Geary TG, Keiser J, Townson S, Harder A, Krücken J.**
668 Characterization of the Ca^{2+} -Gated and Voltage-Dependent K^{+} -Channel Slo-1 of Nematodes
669 and Its Interaction with Emodepside. *PLoS Negl Trop Dis* 8, 2014.

670 **Lee J, Ueda A, Wu C-F.** Distinct roles of *Drosophila* cacophony and Dmca1D Ca^{2+} channels
671 in synaptic homeostasis: Genetic interactions with slowpoke Ca^{2+} -activated BK channels in
672 presynaptic excitability and postsynaptic response. *Dev Neurobiol* 74, 2014.

673 **Lee US, Cui J.** BK channel activation: structural and functional insights. *Trends Neurosci* 33:
674 415–423, 2010.

675 **Lemon WC, Getz WM.** Responses of cockroach antennal lobe projection neurons to
676 pulsatile olfactory stimuli. *Ann N Y Acad Sci* 855: 517–520, 1998.

677 **Lucas P, Shimahara T.** Voltage- and Calcium-activated Currents in Cultured Olfactory
678 Receptor Neurons of Male *Mamestra brassicae* (Lepidoptera). *Chem Senses* 27: 599–610,
679 2002.

680 **Malun D, Waldow U, Kraus D, Boeckh J.** Connections between the deutocerebrum and the
681 protocerebrum, and neuroanatomy of several classes of deutocerebral projection neurons in
682 the brain of male *Periplaneta americana*. *J Comp Neurol* 329: 143–162, 1993.

683 **Mazor O, Laurent G.** Transient Dynamics versus Fixed Points in Odor Representations by
684 Locust Antennal Lobe Projection Neurons. *Neuron* 48: 661–673, 2005.

685 **Mercer AR, Hayashi JH, Hildebrand JG.** Modulatory effects of 5-hydroxytryptamine on
686 voltage-activated currents in cultured antennal lobe neurones of the sphinx moth *Manduca*
687 *sexta*. *J Exp Biol* 198: 613–627, 1995.

688 **Mercer AR, Kloppenburg P, Hildebrand JG.** Serotonin-induced changes in the excitability
689 of cultured antennal-lobe neurons of the sphinx moth *Manduca sexta*. *J Comp Physiol [A]*
690 178: 21–31, 1996.

691 **Nishino H, Yamashita S, Yamazaki Y, Nishikawa M, Yokohari F, Mizunami M.** Projection
692 neurons originating from thermo- and hygro-sensory glomeruli in the antennal lobe of the
693 cockroach. *J Comp Neurol* 455: 40–55, 2003.

694 **Nishino H, Yoritsune A, Mizunami M.** Postembryonic development of sexually dimorphic
695 glomeruli and related interneurons in the cockroach *Periplaneta americana*. *Neurosci Lett*
696 469: 60–64, 2010.

697 **Perk CG, Mercer AR.** Dopamine Modulation of Honey Bee (*Apis mellifera*) Antennal-Lobe
698 Neurons. *J Neurophysiol* 95: 1147–1157, 2006.

699 **Pézier A, Acquistapace A, Renou M, Rospars J-P, Lucas P.** Ca^{2+} Stabilizes the
700 Membrane Potential of Moth Olfactory Receptor Neurons at Rest and Is Essential for Their
701 Fast Repolarization. *Chem Senses* 32: 305–317, 2007.

702 **Pineda JC, Galarraga E, Bargas J, Cristancho M, Aceves J.** Charybdotoxin and apamin
703 sensitivity of the calcium-dependent repolarization and the afterhyperpolarization in
704 neostriatal neurons. *J Neurophysiol* 68: 287–294, 1992.

705 **Pippow A, Husch A, Pouzat C, Kloppenburg P.** Differences of Ca^{2+} handling properties in
706 identified central olfactory neurons of the antennal lobe. *Cell Calcium* 46: 87–98, 2009.

707 **Pym EC, Southall TD, Mee CJ, Brand AH, Baines RA.** The homeobox transcription factor
708 Even-skipped regulates acquisition of electrical properties in *Drosophila* neurons. *Neural*
709 *Develop* 1: 3, 2006.

- 710 **Ryglewski S, Duch C.** Shaker and Shal mediate transient calcium-independent potassium
711 current in a *Drosophila* flight motoneuron. *J Neurophysiol* 102: 3673–3688, 2009.
- 712 **Sah P, Faber ES.** Channels underlying neuronal calcium-activated potassium currents. *Prog*
713 *Neurobiol* 66: 345–353, 2002.
- 714 **Salkoff L, Butler A, Ferreira G, Santi C, Wei A.** High-conductance potassium channels of
715 the SLO family. *Nat Rev Neurosci* 7: 921–931, 2006.
- 716 **Schäfer S, Rosenboom H, Menzel R.** Ionic currents of Kenyon cells from the mushroom
717 body of the honeybee. *J Neurosci* 14: 4600–4612, 1994.
- 718 **Stocker M.** Ca²⁺-activated K⁺ channels: molecular determinants and function of the SK
719 family. *Nat Rev Neurosci* 5: 758–770, 2004.
- 720 **Stopfer M, Jayaraman V, Laurent G.** Intensity versus Identity Coding in an Olfactory
721 System. *Neuron* 39: 991–1004, 2003.
- 722 **Strausfeld NJ, Hildebrand JG.** Olfactory systems: common design, uncommon origins?
723 *Curr Opin Neurobiol* 9: 634–639, 1999.
- 724 **Su C-Y, Menuz K, Carlson JR.** Olfactory Perception: Receptors, Cells, and Circuits. *Cell*
725 139: 45–59, 2009.
- 726 **Vergara C, Latorre R, Marrion NV, Adelman JP.** Calcium-activated potassium channels.
727 *Curr Opin Neurobiol* 8: 321–329, 1998.
- 728 **Vosshall LB, Stocker RF.** Molecular architecture of smell and taste in *Drosophila*. *Annu Rev*
729 *Neurosci* 30: 505–533, 2007.
- 730 **Warren B, Kloppenburg P.** Rapid and slow chemical synaptic interactions of cholinergic
731 projection neurons and GABAergic local interneurons in the insect antennal lobe. *J Neurosci*
732 34: 13039–13046, 2014.
- 733 **Watanabe H, Ai H, Yokohari F.** Spatio-temporal activity patterns of odor-induced
734 synchronized potentials revealed by voltage-sensitive dye imaging and intracellular recording
735 in the antennal lobe of the cockroach. *Front Syst Neurosci* 6: 55, 2012.
- 736 **Watanabe H, Nishino H, Nishikawa M, Mizunami M, Yokohari F.** Complete mapping of
737 glomeruli based on sensory nerve branching pattern in the primary olfactory center of the
738 cockroach *Periplaneta americana*. *J Comp Neurol* 518: 3907–3930, 2010.
- 739 **Wicher D, Walther C, Wicher C.** Non-synaptic ion channels in insects - basic properties of
740 currents and their modulation in neurons and skeletal muscles. *Prog Neurobiol* 64: 431–525,
741 2001.
- 742 **Wilson RI, Mainen ZF.** Early events in olfactory processing. *Annu Rev Neurosci* 29: 163–
743 201, 2006.
- 744 **Wilson RI, Turner GC, Laurent G.** Transformation of olfactory representations in the
745 *Drosophila* antennal lobe. *Science* 303: 366–370, 2004.
- 746 **Wolfart J, Neuheff H, Franz O, Roeper J.** Differential expression of the small-conductance,
747 calcium-activated potassium channel SK3 is critical for pacemaker control in dopaminergic
748 midbrain neurons. *J Neurosci* 21: 3443–3456, 2001.

749 **Yasuyama K, Kitamoto T, Salvaterra PM.** Localization of choline acetyltransferase-
750 expressing neurons in the larval visual system of *Drosophila melanogaster*. *Cell Tissue Res*
751 282: 193–202, 1995.

752 **Yasuyama K, Meinertzhagen IA, Schürmann F-W.** Synaptic organization of the mushroom
753 body calyx in *Drosophila melanogaster*. *J Comp Neurol* 445: 211–226, 2002.

754

FIGURE CAPTIONS

FIG. 1: Morphology of uniglomerular projection neurons and isolation of $I_{K(Ca)}$. *A*: Morphology of the recorded uPN revealed by labeling with biocytin-streptavidin via the patch pipette. *A1*: overview. The neuron innervated a single glomerulus and sent a single axon along the mALT to the mushroom body's calyces (CA) and the lateral horn (LH). The position of the soma, which was lost during processing, is marked (★). *A2-A4*: higher magnification of the framed areas in *A1*. *A1*; *A2*: boutons in the calyces (*A2*) and in the LH (*A3*). *A4*: neurites in the single innervated glomerulus. *B-E*: isolation of $I_{K(Ca)}$. The holding potential was -60 mV. *B*: Currents were activated by 300 ms depolarizing steps from -60 mV to 60 mV in 10 mV increments. *C*: Current traces elicited by the same depolarizing steps as in *B*, during the application of a 5×10^{-4} M Cd^{2+} . *D*: subtraction of the *C* traces from the *B* traces yields $I_{K(Ca)}$. *E*: voltage-dependence for activation of $I_{K(Ca)}$. *I-V* relation and *current density-V* relation of $I_{K(Ca)}$. na, neural anterior; AL, antennal lobe; CA, calyx; GL, glomerulus; mALT, medial antennal lobe tract; l, lateral; LH, lateral horn; ★, soma location.

FIG. 2: Voltage-dependence of $I_{K(Ca)}$. *A*: *I-V* relation. *B*: *current density-V* relation. Current density was calculated from the ratio between $I_{K(Ca)}$ and the cell capacitance. *C,D*: normalized *I-V* relation ($I_{K(Ca)}$ as fractions of the maximal $I_{K(Ca)}$ for each neuron). *A-C* are based on the same original recordings with $[Ca^{2+}]_o = 1$ mM. The recordings in *D* were performed in $[Ca^{2+}]_o = 6$ mM. Gray: individual cells; black: mean \pm SD.

FIG. 3: $I_{K(Ca)}$ is dependent on the amplitude and duration of the " Ca^{2+} loading-pulses". Test pulses depolarized the membrane to +60 mV where virtually no voltage activated Ca^{2+} influx occurs, since the membrane approaches the Ca^{2+} equilibrium potential. The test pulses were preceded by " Ca^{2+} loading-pulses" of varying amplitude (*A1-A4*) or duration (*B1-B3*). *A1-A4*:

the +60 mV test pulses were preceded by 200 ms depolarizing Ca^{2+} loading-pulses of varying amplitude (-60 mV to +60 mV; 10 mV increments). *A1*: currents in response to the +60 mV test pulse preceded by loading-pulses to +10 mV (large Ca^{2+} influx) and to +60mV (virtually no Ca^{2+} influx). *A2*: same experiment as in *A1* with the whole series of loading-pulses from -60 mV to +60 mV. *A3*: framed area of *A2* in higher resolution. *A4*: I - V_{loading} relation of $I_{\text{K(Ca)}}$. The I - V_{loading} relation shows $I_{\text{K(Ca)}}$ at the beginning of the +60 mV test pulse plotted as a function of the loading-pulse voltage. *B1-B3*: the +60 mV test pulses were preceded by Ca^{2+} loading-pulses of varying duration (5 ms – 400ms). The loading-pulse amplitude was adjusted for each neuron to values where maximal loading occurred during the first part of the experiments (see *A4*). *B1*: currents in response to the + 60 mV test pulse that were preceded by 10 mV loading-pulses of varying duration. *B2*: $I_{\text{K(Ca)}}$ at the beginning of the +60 mV test pulses (normalized to the maximal $I_{\text{K(Ca)}}$ of each cell) plotted as a function of the loading-pulse duration. *B3*: The decay time constant of $I_{\text{K(Ca)}}$ in dependence of the loading-pulse duration.

FIG. 4: Voltage and Ca^{2+} dependence of $I_{\text{K(Ca)}}$. To measure the voltage and Ca^{2+} dependence of $I_{\text{K(Ca)}}$ independently from the instantaneous Ca^{2+} influx, $I_{\text{K(Ca)}}$ was recorded under voltage and $[\text{Ca}^{2+}]_{\text{i}}$ clamp. The holding potential was -60 mV and voltage pulses were applied between -60 mV and +90 mV in 10 mV increments. The cytosolic Ca^{2+} concentration $[\text{Ca}^{2+}]_{\text{i}}$ was clamped at 56 μM (n=5), 143 μM (n=5), mM, 540 μM (n=6) or 1800 μM (n=6) using an EDTA or EGTA - Ca^{2+} buffering system. Voltage activated Ca^{2+} currents were blocked by 5×10^{-4} M CdCl_2 . *A*: Under clamped $[\text{Ca}^{2+}]_{\text{i}}$ $I_{\text{K(Ca)}}$ did not inactivate during a sustained voltage pulse. Increasing Ca^{2+} concentrations increased the $I_{\text{K(Ca)}}$ amplitude and at all Ca^{2+} concentrations $I_{\text{K(Ca)}}$ increased with increasing depolarization. *B*: Example traces (different neurons) demonstrating the effect of increasing $[\text{Ca}^{2+}]_{\text{i}}$ on $I_{\text{K(Ca)}}$. *C*: G - V relations for different $[\text{Ca}^{2+}]_{\text{i}}$. Error bars are omitted for better visualization. *D*: Voltages for half-maximal activation ($V_{0.5,\text{act}}$) for different $[\text{Ca}^{2+}]_{\text{i}}$.

808

809 FIG. 5: Charybdotoxin and iberiotoxin reduce $I_{K(Ca)}$. *A*: Example traces (different neurons)
810 demonstrating the effect of increasing concentrations of CTX (left) and IbTX (right) on $I_{K(Ca)}$.
811 *B*: *Concentration - response* relation of CTX and IbTX. The curves are fits to a sigmoidal
812 relation (*Eq. 1*). CTX had an IC_{50} of 2.7 nM (1.8 nM – 3.8 nM) and IbTX had an IC_{50} of 157
813 pM (53.7 pM - 460 pM).

814

815 FIG. 6: Uniglomerular projection neurons do not generate I_{SK} . *A*: In dopaminergic substantia
816 nigra neurons of mice a short depolarizing voltage pulse (Ca^{2+} loading-pulse), evoked Ca^{2+}
817 influx which activated an apamin sensitive I_{SK} . *B*: uPNs did not generate I_{SK} . The 100 ms
818 loading-pulse to 0 mV was preceded by a 1 s hyperpolarizing step to -80 mV. The holding
819 potential was -60 mV. The recordings are only shown for the framed region of the voltage
820 protocol. p/n protocols were not applied. The apamin concentration was 100 nM in *A* and 1
821 μ M in *B*.

822

823 FIG. 7: Comparison of direct and indirect "block" of $I_{K(Ca)}$ by CTX and Cd^{2+} respectively. The
824 holding potential in all recordings was -60 mV. Currents were activated by 300 ms
825 depolarizing steps from -60 mV to +60 mV in 10 mV increments. *A*: whole cell currents of a
826 uPN during TTX and 4-AP application. *B,C*: recordings of the same neuron as in *A*, during
827 the additional application of CTX (*B*) and during the application of CTX and 5×10^{-4} M Cd^{2+}
828 (*C*). *D*: Subtraction of the *B* traces from the *A* traces. *E*: Subtraction of the *C* traces from the
829 *B* traces. *F*: *I-V* relation for the current traces shown in *A-E*.

830

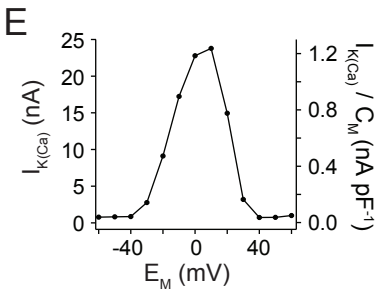
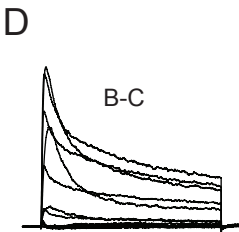
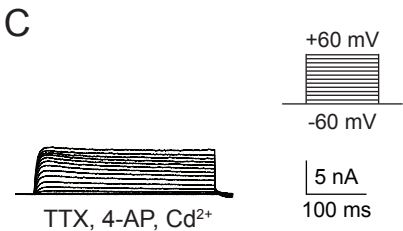
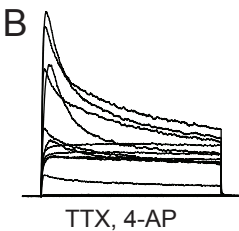
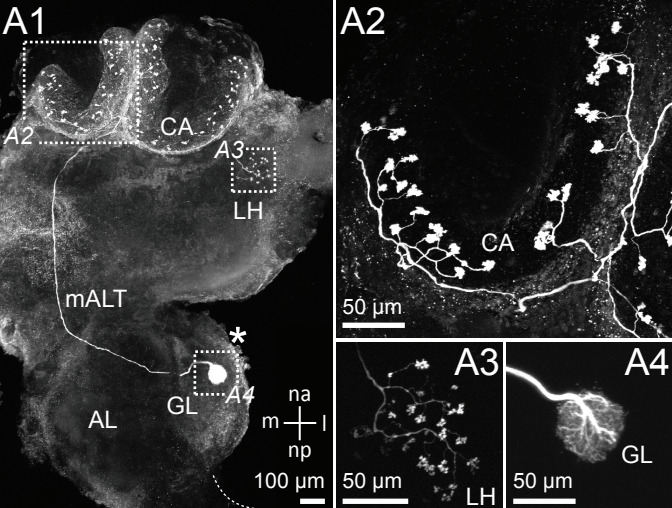
831 Fig. 8: Example current clamp recording to demonstrate the CTX effect on action potential
832 waveform.

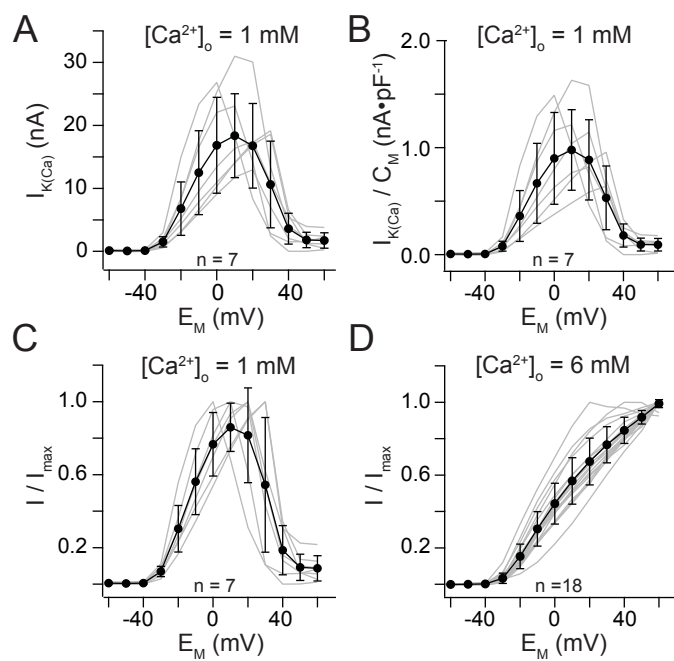
833

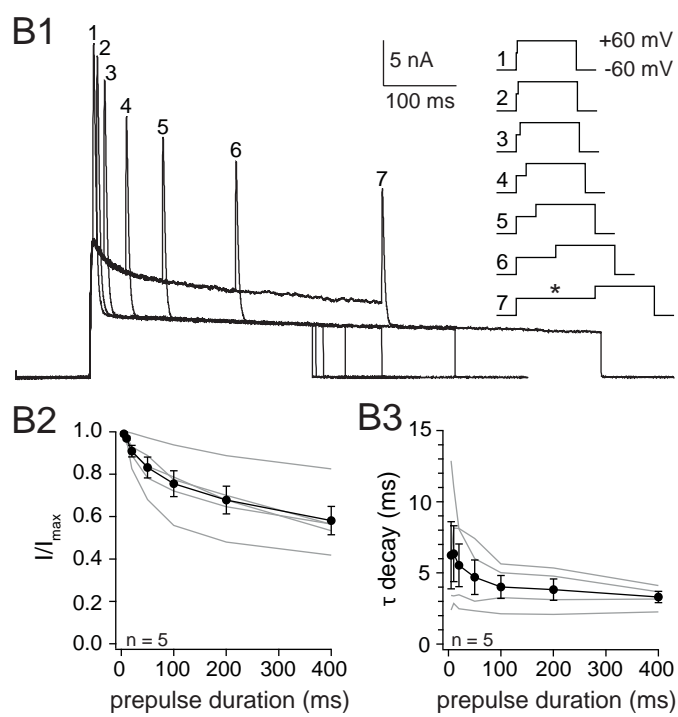
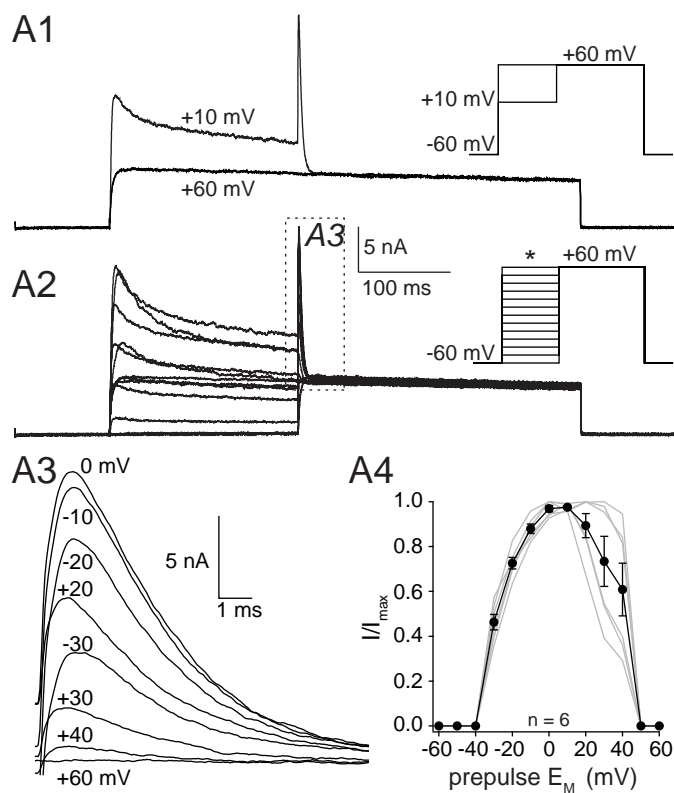
834 FIG. 9: Summary and quantification of the charybdotoxin (*A*), iberiotoxin (*B*), and apamin (*C*)
835 effects on electrophysiological properties (rate of repolarization [1], amplitude of
836 afterhyperpolarization [2], width of half maximal amplitude [3], latency to first action potential
837 during a depolarizing voltage step [4], action potential threshold [5], and number of action
838 potentials during 500 ms depolarizing current pulses [6]). The schematics demonstrate how
839 the parameters were measured; for details see METHODS. n values are given in the bars of
840 each graph. * ≤ 0.05 ; ** ≤ 0.01 ; *** ≤ 0.001 . Apa, apamin; CTL, control; CTX, charybdotoxin;
841 IbTX, iberiotoxin; W, wash.

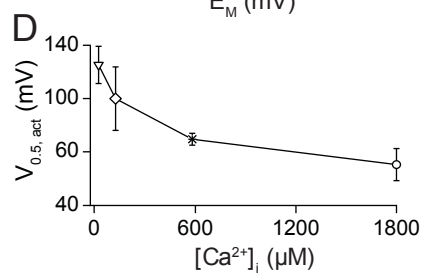
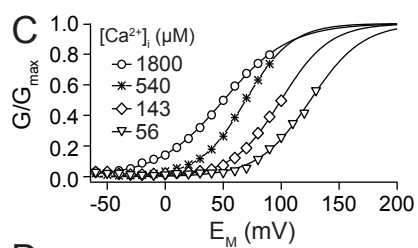
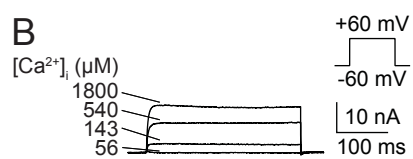
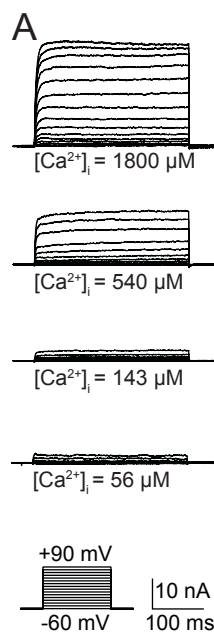
842

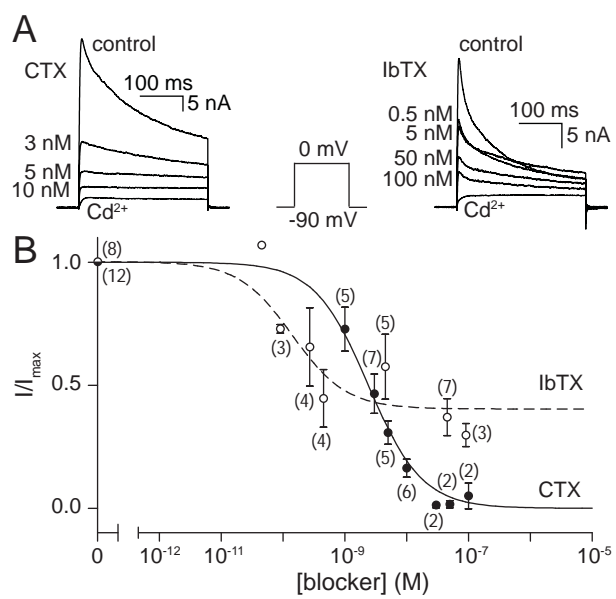
843

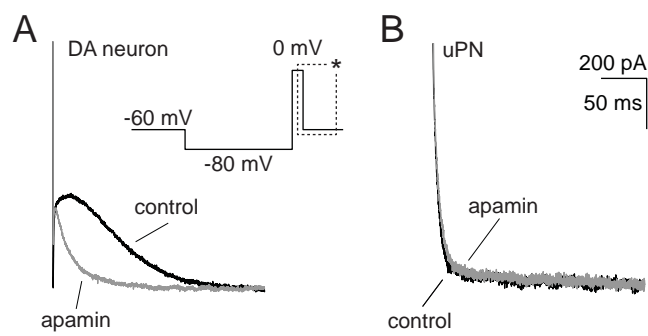


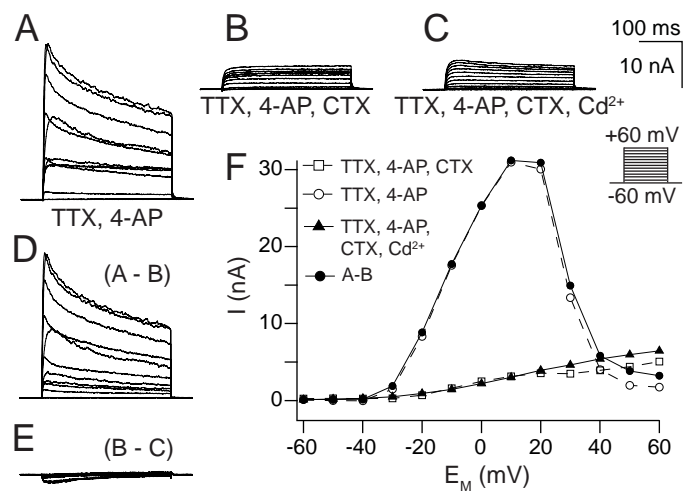


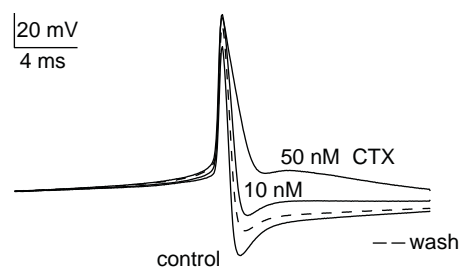




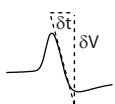








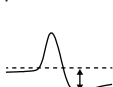
repolarisation
rate



width



afterhyper-
polarisation



latency



threshold

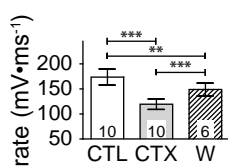


firing

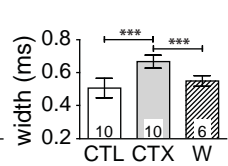


Charybdotoxin

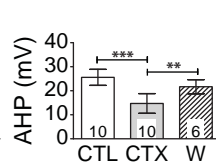
A1



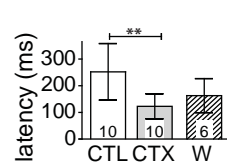
A2



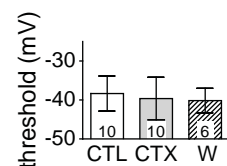
A3



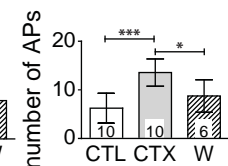
A4



A5

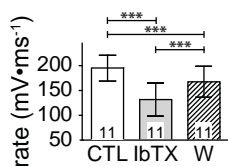


A6

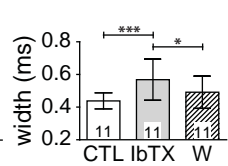


Iberitoxin

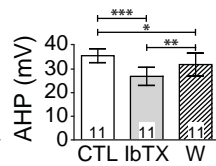
B1



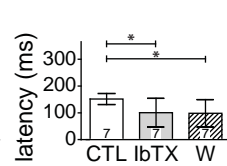
B2



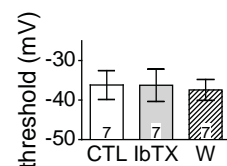
B3



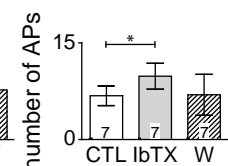
B4



B5

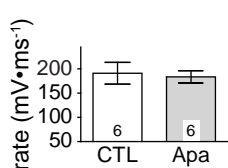


B6

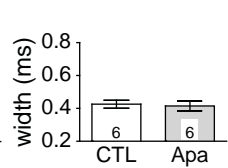


Apamin

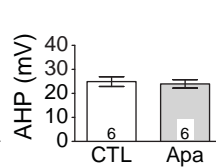
C1



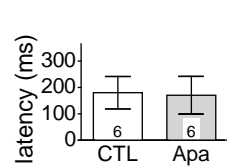
C2



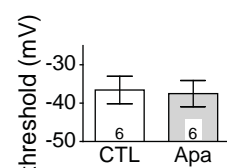
C3



C4



C5



C6

